

# **DEM based deterministic landslide hazard analysis in the Lesser Himalaya of Nepal**

Ranjan Kumar Dahal. Shuichi Hasegawa. Atsuko Nonomura. Minoru Yamanaka. Santosh Dhakal

R. K. Dahal\*

*1 Dept. of Safety Systems Construction Engineering, Faculty of Engineering, Kagawa University, 2217-20, Hayashi-cho, Takamatsu City, 761-0396, Japan*

*2 Department of Geology, Tri-Chandra Multiple Campus, Tribhuvan University, Ghantaghar, Kathmandu, Nepal*

S. Hasegawa . A. Nonomura . M. Yamanaka

*Dept. of Safety Systems Construction Engineering, Faculty of Engineering, Kagawa University, 2217-20, Hayashi-cho, Takamatsu City, 761-0396, Japan*

Santosh Dhakal

*Department of Mines and Geology, Lainchaur, Kathmandu, Nepal*

\*Corresponding author's email: ranjan@ranjan.net.np, Fax: 0081-87-864-2031 (O), Phone: 0081-87-864-2140 (O), Mobile: 0081-90-6289-2496

**Cite this article as:** Dahal R.K., Hasegawa S., Nonomura A., Yamanaka M., Dhakal S., 2008, DEM-based deterministic landslide hazard analysis in the Lesser Himalaya of Nepal, *Georisk: Assessment and Management of Risk for Engineered Systems and Geohazards*, 2(3):161-178. DOI:10.1080/17499510802285379

## **Abstract**

In Nepal, people live in widely spread settlements in the fragile Himalayan terrains, and suffer more from landslides than from any other type of natural disaster. The small-scale rainfall-triggered landslides in the Lesser Himalaya of Nepal are generally shallow (about 0.5 to 2.5 m) and are triggered by changes in the physical property of soil layers during rainfall. The relation between landslides and slope hydrology has received little attention in Himalayan landslide research. Thus, this paper deals with the probability of slope failure during extreme rainfall events by considering a Digital Elevation Model (DEM)-based hydrological model for soil saturation depth and an infinite slope stability model. Deterministic distributed analysis in GIS was carried out to calculate the probability of slope failure. A simple method of error propagation was used to calculate the variance of the safety factors and the probability of failure. When normally distributed failure probability values were checked against existing landslides, it was found that more than 50% of the pixels of existing landslides coincided with a high calculated probability of failure. Although the deterministic distributed analysis has certain drawbacks, as described by previous researchers, this study concluded that the calculated failure probability can be utilized to predict the probability of slope failure in Himalayan terrain during extreme rainfall events.

# 1 Introduction

Landslides are very common in Himalayan terrain. Intense summer monsoons are the main trigger for landslides. Every year, especially during monsoon periods, tremendous damage to lives, property, infrastructure, and the environment in Nepal is caused by landslides and related natural events. In the fragile Himalayan terrains of Nepal, people live in widely spread settlements and suffer more from landslides than from any other type of natural disaster. A large number of human settlements on the Nepalese mountains and hills of Lesser Himalaya are situated either on old landslide mass or on landslide-prone areas. Because of this, a great number of people are affected by large- and small-scale landslides all over Nepal, especially during monsoon periods. The small-scale rainfall-triggered landslides in Nepal are generally shallow (about 0.5 to 2.5 m) and are triggered by changes in the physical properties of soil layers during rainfall (Upreti and Dhital, 1996; Dahal and Hasegawa, 2008). The relation between landslides and slope hydrology has received little attention in research on Himalayan landslides. It is therefore important to assess the hydrological response of slopes with respect to slope materials and morphology.

Although, it is difficult to assess the hydrological response of a slope during rainfall, many studies have noted the importance of the relationship between topography, hydrology and slope materials for rainfall-triggered landslides (Beven and Kirkby 1979; Ward et al. 1981; Iida 1984; Okimura and Kawatani 1987; Montgomery and Dietrich 1994; Wu and Sidle 1995; Dietrich et al. 1995; Burton and Bathurst 1998; Borga et al. 1998; Lamb et al. 1998; Borga et al. 2002; Pack et al. 1998, 2001; Crozier 1999; Iida 1999; Iverson 2000; Glade et al. 2000; Duzgun et al. 2003; Xie et al. 2004; Can et al. 2005; among others). A successful approach to modelling the influence of topography on slope material saturation behaviour was established by Beven and Kirkby (1979), in the form of a topography index. This model was incorporated successfully into a hydrological model known as TOPMODEL, which simulated runoff hydrographs (Lamb et al. 1998). Iida (1984) developed a hydrological model of slope in terms of topographic effect, saturated through flow, and rainfall timing. This model provides a framework for interpreting topographic effect in steep soil-mantled slopes for the preliminary identification of slopes that are prone to experiencing shallow landslides during extreme rainfall events. Okimura and Kawatani (1987) developed a hydrological model by using the finite difference method and Darcy's Law to solve the Laplace equation for saturated transient flow. They applied the model successfully to granitic terrain in Japan. Dietrich et al. (1995) and Montgomery and Dietrich (1994) developed a contour- or polygon-based hill slope hydrological model called SHALSTAB. This model also considers some of the index properties of slope materials. However, it assumes that during slope failure, slope materials have no cohesion. This model can be implemented as an extension of commercially available GIS software (ArcView). Pack et al. (1998, 2001) developed another approach to modelling (SINMAP), which is suitable for applying to slopes that have a shallow soil depth and impermeable underlying bedrock. It is similar to SHALSTAB, but uses cohesion and root cohesion (for forested slope) in calculation. Thus, SINMAP may be viewed as an advanced version of SHALSTAB. The contributing area is one of the important topographic parameters used in SINMAP. This model can be also implemented as an extension of ArcView. Iida (1999) emphasized the deterministic and stochastic aspects of the shallow landslide prediction

model. The model described by Iverson (2000) illustrates the infiltration process of rainfall and landslide processes. He showed that the use of pressure head response, topographic data, rainfall intensity and duration, along with infinite-slope failure criteria, helps to predict the timing, depth, and acceleration of rainfall-triggered landslides. The Antecedent Soil Water Status Model (ASWSM) described by Crozer (1999) and Glade et al. (2000) accounts for the draining of early rainfall and accumulation of late rainfall. They provide an equation for estimating the probability of landslide occurrence as a function of daily intensity and previous water accumulation.

The aim of the study reported herein was to find and deploy a simple analytical method that can be used to explain the probability of failure in marginal hills of settlements in the Lesser Himalayan terrain during monsoon rainfall. To this end, the probability of slope failure in the south-western hills of Kathmandu, Lesser Himalaya in the GIS platform was evaluated by using the criteria for infinite slope failure and topographically-based hydrological model described by Iida (1984).

## **2 The deterministic model**

Over the last 40 years, many researches have been done to analyze the probability of slope failure and the risk of landslides. These research methods are mainly orientated towards site investigation and analysis using the deterministic distributed model approach (Graham 1984, Montgomery and Dietrich 1994, van Westen and Terlien 1996, Terlien et al. 1995, Gökceoglu and Aksoy 1999, Duzgun et al. 2003; Acharya et al., 2006, among others). The deterministic or physically based models are based on the physical laws of conservation of mass, energy and momentum (van Westen and Terlien 1996, Terlien et al. 1995). Many deterministic models are site-specific and do not consider the spatial distribution of the input parameters. However, the deterministic distributed model takes into account the spatial distribution of parameters in the GIS platform. This model is mainly used to analyze the probability of landslide when a terrain consists of homogeneous geology and geomorphology (van Westen and Terlien 1996).

A one-dimensional infinite slope stability model (Skepton and DeLory 1957, Graham 1984, Hammond et al. 1992, Duncan 1996) is often used when analysing stability and calculating factors of safety when using deterministic distributed modelling in GIS. This method is applicable when the thickness of the soil mantle is much less than the length of the slope and where the failure plane is approximately parallel to the slope surface. Although there are some constraints on the use of the deterministic model by one-dimensional infinite slope stability modelling in comparison to two- and three- dimensional modelling (van Westen and Terlien 1995, Xie et al 2004), the model can calculate slope instability on a pixel basis and is very suitable for use in raster GIS (Wards et al., 1981, Okimura and Kawatani 1987, Hammond et al. 1992, van Westen and Terlien 1995, Terlien 1996, van Westen 2000, Soeters and van Westen 1996). The one-dimensional infinite slope stability model needs resilient information about hill slope hydrology during deterministic analysis (Hammond et al. 1992, Borga et al., 1998). Thus, it is necessary to explain the infinite slope stability model coupled with the hydrological model before conducting deterministic analysis in the GIS platform.

A detailed flow chart of research is illustrated in **Figure 1**. The flow of research mainly includes field work, digital data processing and laboratory analysis to obtain all parameter required for coupled infinite slope stability and hydrological model. Review of available literatures and procurement of data from previous works were also done in the preliminary phase of research. Soil mapping, land use mapping, insitu test were main work out of field study. Digital data processing mainly includes DEM based parameterization for modelling. Average factor of safety map were prepared and variance of safety factor was calculated. Finally, probability maps of various rainfall scenarios were calculated. The details of the one-dimensional infinite slope stability model coupled with hydrological model are discussed below.

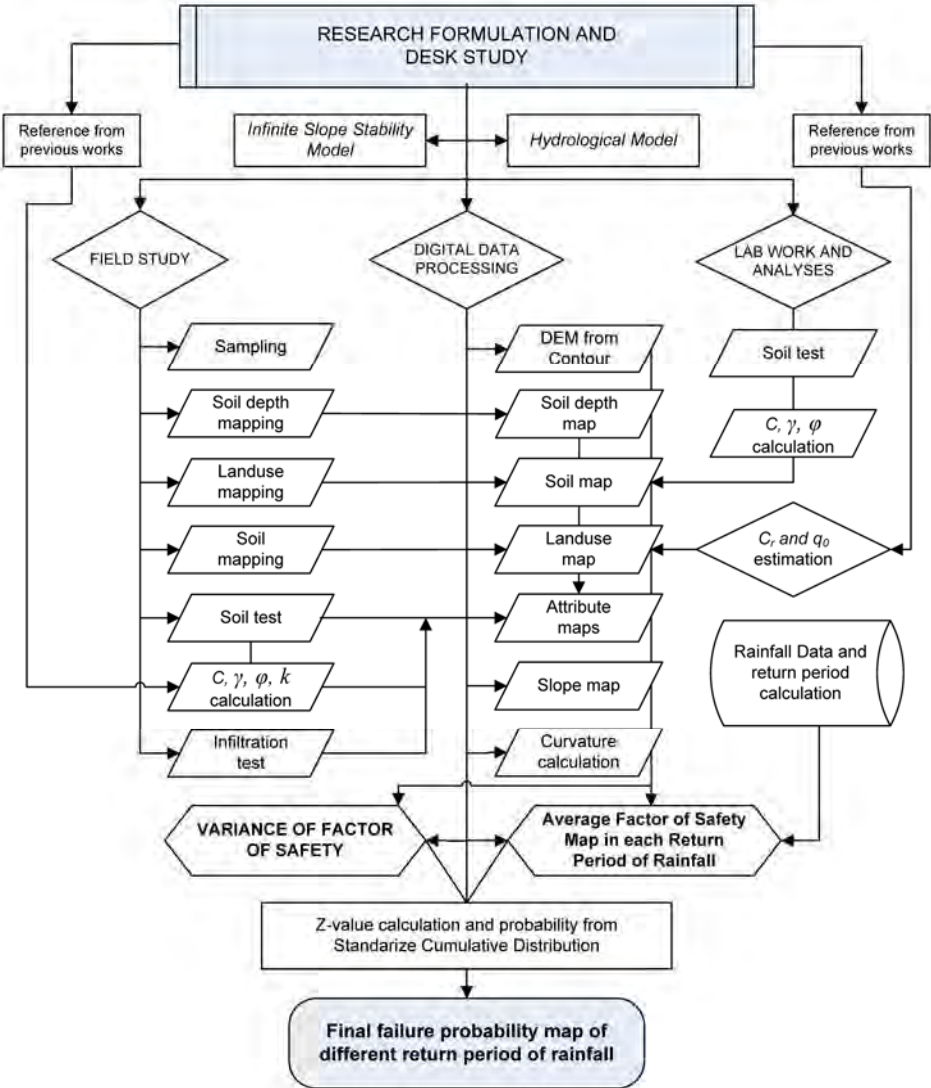


**Figure 1** Framework of the study

## 2.1 Stability and hydrological models

The infinite slope stability model depends on several assumptions (Skepton and DeLory 1957, Hammond et al. 1992, Duncan 1996). The mathematical simplicity that results from the assumptions makes infinite slope analysis uniquely well suited for drawing explicit conclusions about the effects of hill slope hydrology on slope stability (Ward et al., 1981, Okimura and Kawatani 1987, Iverson 2000, Borga et al. 2002). For the implementation of the coupled stability and hydrological models, the following assumptions were made:

- The infiltration capacity of the soil always exceeds the rainfall intensity, so that the Hortonian overland flow is ignored and groundwater table rises when the rainfall infiltrates.
- Hydraulic conductivity is assumed to be uniform in soil
- Constant intensity of rainfall and saturated through flow parallel to bedrock are assumed.
- Steady-state conditions are considered to apply, so the through flow rate is proportional to the recharge.
- Flow from or inside bedrock (Onda 1992) is not considered

For an infinite slope (Figure 2), the factor of safety is calculated as follows (for example, Okimura and Kawatani 1986, Hammond et al. 1992):

$$FS = \frac{C + C_r + A \cos^2 \beta \tan \phi}{B \sin \beta \cos \beta} \dots \dots \dots (1)$$

In which

$$A = q_0 + h (\gamma_{sat} - \gamma_w) + \gamma_t (D - h) \dots \dots \dots (2)$$

$$B = q_0 + h \gamma_{sat} + \gamma_t (D - h) \dots \dots \dots (3)$$

Where  $FS$  is the factor of safety,  $C$  is soil cohesion ( $\text{kN/m}^2$ ),  $C_r$  is effective root strength,  $\phi$  is the internal friction angle of the soil (degrees),  $q_0$  is the vegetation surcharge per unit area ( $\text{kN/m}^2$ ),  $\gamma$  is the unit weight of soil ( $\text{kN/m}^3$ ),  $\gamma_{sat}$  is the saturated unit weight of soil ( $\text{kN/m}^3$ ),  $\gamma_w$  is the unit weight of water ( $\text{kN/m}^3$ ),  $D$  is the depth of the soil layer above the bedrock surface (m),  $h$  is the saturated depth of soil (m), and  $\beta$  is slope inclination (degrees).

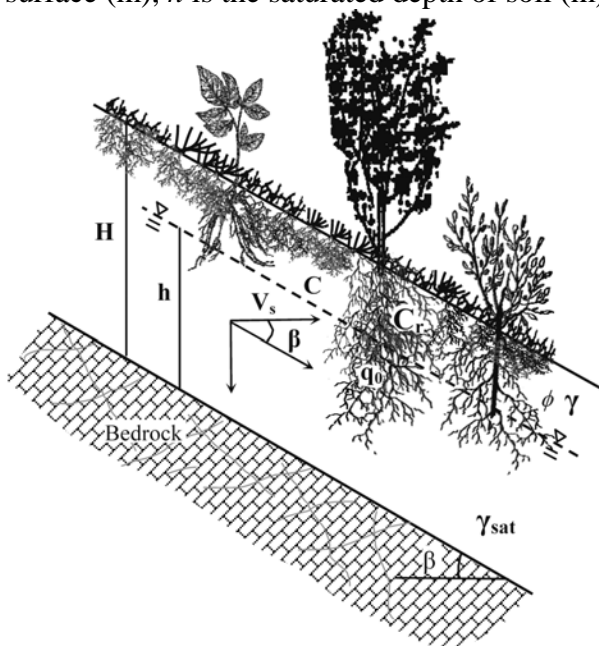


**Figure 2** Infinite slope stability model

In a theoretical hydrological model of saturated through flow during rainfall, Iida (1984) assumed that saturated through flow in the soil layer moves down along a flow line as per Darcy's law. He introduced a horizontal component of flow velocity and expressed it in terms of saturated hydraulic conductivity and effective porosity as follows.

Referring to **Figure 2**,

$$q' = k \sin\beta \dots\dots\dots (4)$$

$$V_s = \frac{k}{n} \sin\beta \cos\beta \dots\dots\dots (5)$$

Where  $q'$  is specific flux (m/s),  $k$  is saturated hydraulic conductivity (m/s), and  $n$  is effective porosity and  $V_s$  is horizontal component of interstitial velocity. Iida also described through flow travel time from one point to another on a slope. If  $u$  and  $v$  are two points on a slope (**Figure 3**), the travel time from  $u$  to  $v$  can be expressed as follows:

$$t_{uv} = \int_u^v \frac{1}{V_s} ds \dots\dots\dots (6)$$

Now, from Equations 4 and 5,

$$t_{uv} = \frac{n}{k} \int_u^v \frac{1}{\sin\beta \cos\beta} ds \dots\dots\dots (7)$$

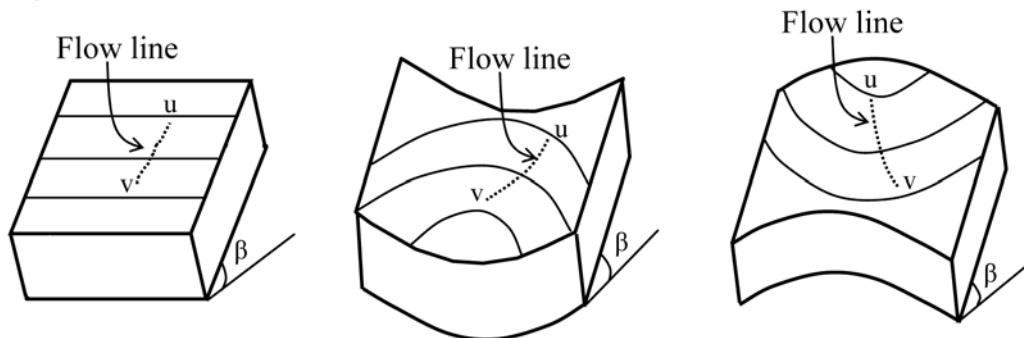


**Figure 3**, Schematic illustration of saturated flow in soil layer in planar, concave and convex slopes as defined by Iida (1984)

Where,  $t_{uv}$  is the travel time and  $s$  is the horizontal distance between  $u$  and  $v$ . A barrier with length  $\Delta l$  is assumed to lie parallel to the contour line at any point on the slope. Isolines of the time required for water to reach the barrier can be explained on the upslope. Iida stated that an area surrounded by the barrier, two watershed lines, and an isoline at time  $t$  can be obtained as a function of  $t$ . He conclusively defined the curve of the specific surrounded area,  $a(t)$ , as a function of the travel time  $t$  and the status of rainfall of constant intensity in time  $t$  expressed in terms of the surrounding area,  $a(t)$ , discharge per unit area,  $Q(t)$  and saturated depth,  $H(t)$  as follows:

$$Q(t) = R a(t) \dots\dots\dots (8)$$

$$H(t) = \frac{R a(t)}{k \sin\beta \cos\beta} \dots\dots\dots (9)$$

Where,  $R$  is the total rainfall (total rainfall >> the constant rainfall intensity) in time  $t$ .

On an idealized slope that has constant inclination, Iida expressed  $a(t)$ ,  $Q(t)$  and  $H(t)$  as the curvature of the barrier,  $\varepsilon$ , as follows:

$$a(t) = t V_s \left[ 1 + \left( \frac{\varepsilon}{2} \right) V_s t \right] \dots\dots\dots (10)$$

$$Q(t) = R V_s \left[ t + \left( \frac{\varepsilon}{2} \right) V_s t^2 \right] \dots\dots\dots (11)$$

$$H(t) = \frac{R}{n} \left[ t + \left( \frac{\varepsilon}{2} \right) V_s t^2 \right] \dots\dots\dots (12)$$

The value of  $\varepsilon$  is positive for a concave slope, negative for a convex slope and zero for a planar slope. Equation (12) illustrates the soil saturation at point u (Figure 3) in travel time  $t$ . The law of conservation of mass allows us to consider the travel time  $t$  as being equal to the duration of rainfall and the theoretical model illustrate by Iida (1984) can be utilized to estimate the saturation depth of soil on a slope during total effective rainfall. Because of the advanced development of GIS applications, nowadays it is quite possible to the calculate curvature,  $\varepsilon$ , on every slope unit of a natural slope. Such slope units are termed “unit cells” or “pixels” in GIS and have constant inclination. In raster GIS, the curvature,  $\varepsilon$ , can be derived from the following relationship (Uchida et al., 2004):

$$\varepsilon = \frac{\frac{\partial^2 f}{\partial x^2} \left\{ 1 + \left( \frac{\partial f}{\partial y} \right)^2 \right\} + \frac{\partial^2 f}{\partial y^2} \left\{ 1 + \left( \frac{\partial f}{\partial x} \right)^2 \right\} - 2 \frac{\partial f}{\partial x} \frac{\partial f}{\partial y} \frac{\partial^2 f}{\partial x \partial y}}{\sqrt{2 \left( 1 + \left( \frac{\partial f}{\partial x} \right)^2 + \left( \frac{\partial f}{\partial y} \right)^2 \right)^3}} \dots\dots\dots (13)$$

Where  $f$  is the pixel value of a DEM generated from the contour map, and  $x$  and  $y$  are values of the local coordinate system.

From Equations (1), (12) and (13), hydrological and stability models were established and were used to estimate the factors of safety in each pixel for various effective durations of rainfall.

### 3 The study area

The study area is located in the south-western hills of the Kathmandu valley, Lesser Himalaya, Nepal (Figure 4). The Kathmandu valley is a largest intermountain basin of Lesser Himalayan Zone of the Himalaya that is surrounded by high rising mountain ranges. The study area belongs to Lesser Himalayan Zone of Himalaya (Gansser, 1964) situated close to the central part of Nepal and it consists of the Phulchauki and Bhimphedi groups (which together form the Kathmandu Complex) and is formed by Precambrian to Devonian rocks (Stöcklin 1980). The Bhimphedi Group consists of relatively high-grade metamorphic rocks of Precambrian age, whereas the Phulchowki Group is comprised of weakly metamorphosed sediments of early to middle Palaeozoic age. The rock consists of intensely folded and faulted metasediments, such as phyllites, schists, slates, limestone and marbles. The southern hills of the Kathmandu valley consist mainly of limestone and a subordinate amount of shale and sandstone of the Phulchauki Group (Figure 5).

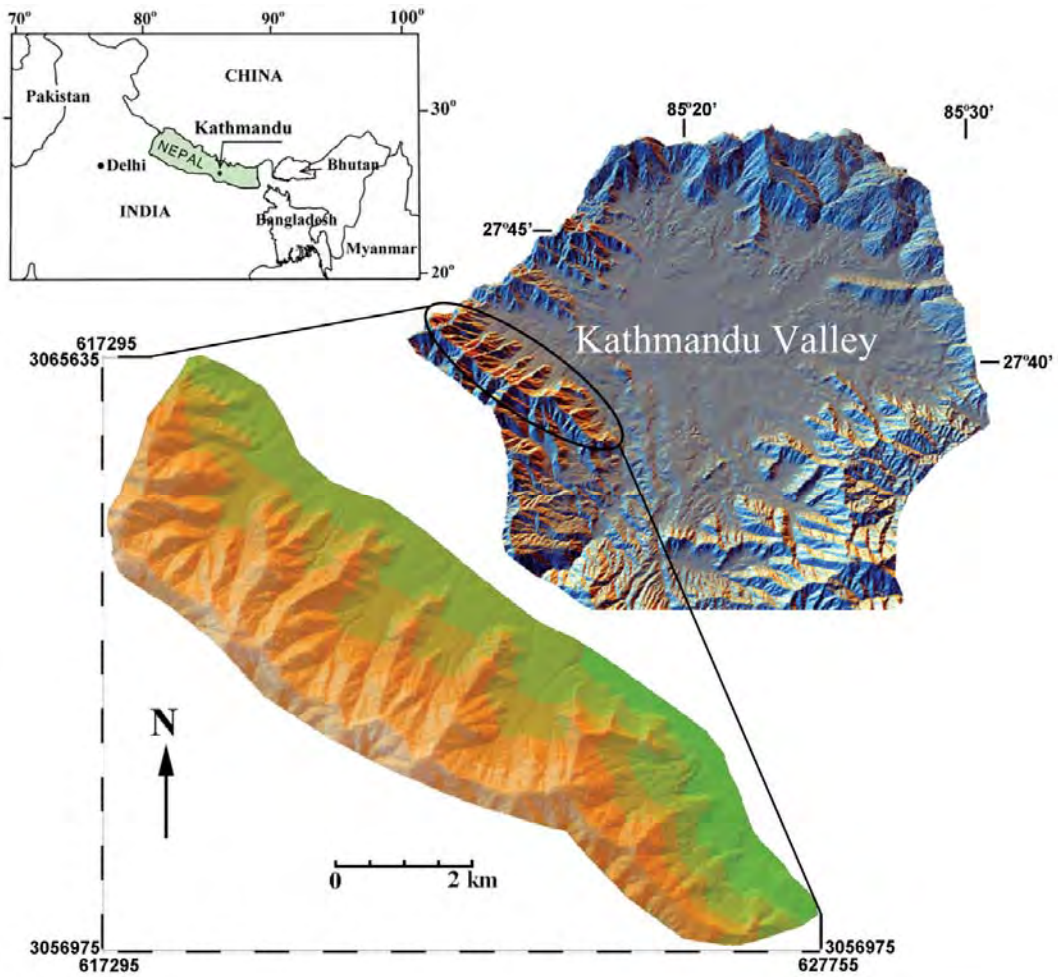


**Figure 4** Location of the study area

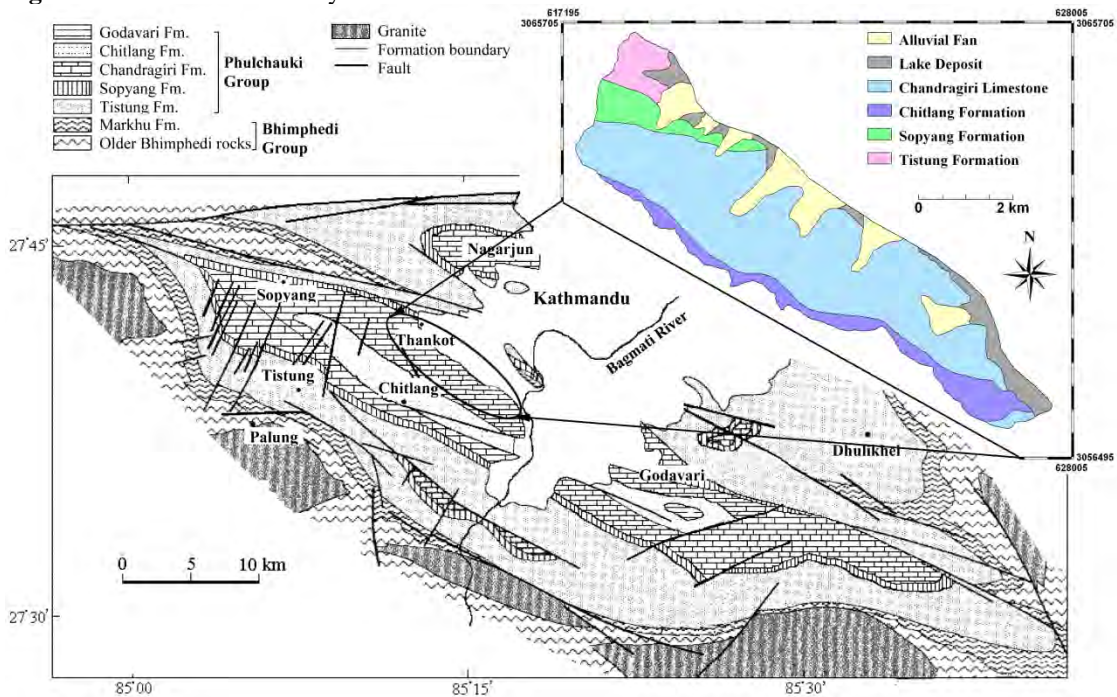


**Figure 5** Geological map of Kathmandu valley area (modified after Stöcklin 1980) and inset illustrates detail geological map of the study area

Colluvial soil is the main slope material above the bedrock. Until 20 years ago, the area was critically deforested, but since then, the area has been reforested and is protected by the local communities. However, the newly planted trees are still not mature; at present, the area consists mainly of a dense forest of immature trees and thorny shrubs. The area is on the outskirts of Kathmandu Metropolitan city in Nepal, and settlement on the base of hills has risen sharply over the last 10 years. Because of the panoramic view of the Himalayas to the north, many housing projects have been started on the base of hills without any consideration of landslide hazards. In the study area, according to classification proposed by Cruden and Varnes (1996), mainly translational sense of movement was noticed in all failures. However, in some slides, after detachment, the failed materials were transported to the base of hills in the form of debris flow. In 2002, a single landslide occurred near the central part of the study area, killing 16 people who were living at the base of the hill (Dahal and Kafle 2003). It was one of the worst natural disasters of that area in the last 50 years and there is a threat of further disasters. A certain amount of research has been conducted that pertains to landslides, and the risk of their occurrence, in the study area. Paudel (2003) described a disaster management scenario for the central part of the study area, giving examples of the disastrous landslides of 2002. Paudyal and Dhital (2005) used the InfoVal method to perform a statistical analysis of risk for the southern part of Kathmandu, including the study area, and categorized the levels of risk as low, moderate and high. Dahal et al. (2006) provided a comprehensive description of the study area with respect to the issue of rainfall and landslides. Dahal et al. (2008) did predictive modelling of landslide hazard for the study area with the weights-of evidence modelling.

### ***3.1 Data procurement***

#### ***3.1.1 Rainfall***

The maximum precipitation in one day was considered to be effective rainfall for the purpose of analysing the probability of failure. The nearest rainfall station to the study area is at Thankot. It was established in 1967 and is only 1.5 km from the study area. In total, 38 years of data were used to calculate the return period of maximum one-day rainfall. The maximum and minimum one day rainfall of study area is 300.1 in the year 2002 and 41.3 in the year 1982, respectively (Figure 6). In July 23, 2002, rainfall of 300.1 mm was accumulated in 24 hours and extensive damage occurred in the study area. In 2002 July, before the day of failure (i.e. 23 July, 2002), the antecedent rainfall of seven days was only 166 mm and for the Lesser Himalaya of Nepal, it is usually a normal antecedent rainfall of the monsoon season (Dahal and Hasegawa, 2008).

The return period was estimated using DISTRIB 2.13 (Eaglin 1996) available with SMADA 6.43 software package (Wanielista et al. 1996). Return periods of 2-, 5-, 10- and 25-years, along with the maximum one-day rainfall of 2002 (which was responsible for triggering numerous recent landslides in the study area), were used for analysing the probability of failure.

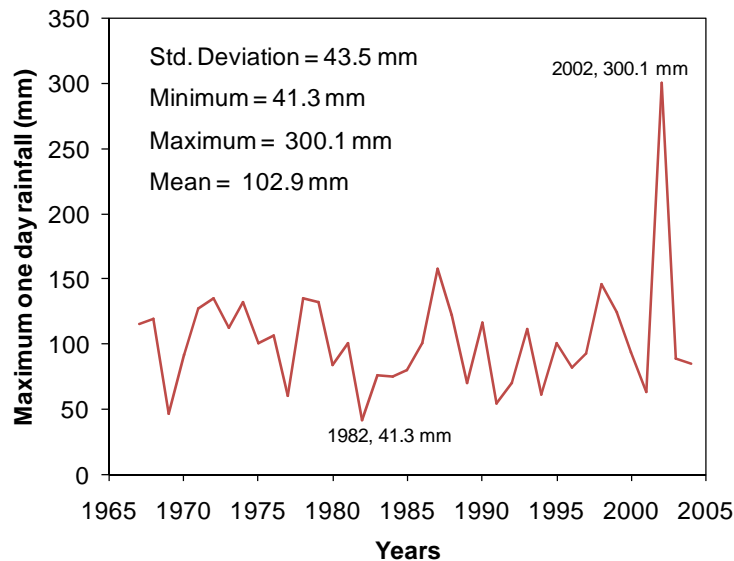


**Figure 6** Trend of maximum one day rainfall in the study area, data of 38 years (1967 to 2004) were used in the analysis

The return period of maximum one-day rainfall were calculated by Pearson Type III, Log Pearson Type II and Gumbel Type 1 Extremal distribution methods. The results are given in **Table 1**. The Pearson Type III distribution method yielded the greatest amount and so return period calculated from Pearson Type III distribution method was used for analysing the probability of slope failure.

### 3.1.2 Field data collection

Field investigations were conducted to gather information about geology, soil type, soil depth, engineering soil type, land use, and to perform in situ tests. For the geology of the study area, previous studies (Stöcklin and Bhattarai 1977, Acharya 2001) were consulted and geological boundaries and structures were checked and modified as per the field observations.

Soil mappings were performed mainly for estimating soil depth and identifying engineering soil types. For this purpose, the study area was divided into 16 topographical mosaics, i.e., more or less homogeneous topographic units, on the basis of the orientation of contour lines and similar geomorphological setting. Field observations suggested that these mosaics usually had approximately homogeneous soil thickness in transverse section. Thus, for the estimation of soil depth within each topographic mosaic, 29 longitudinal profile lines were fixed with respect to increments of height from down slope to upslope of each mosaic. Depending upon the variations of soil thickness in longitudinal section of mosaic, maximum three profiles and minimum one profile were prepared in each mosaic (**Figure 7**). In addition, measurements and observations of soil depth were made at random during field visits. More than 400 observations and estimations (in both cross sections and random points) were made for this purpose and point map of soil depth were prepared in a topographical map of 1:25 000 scale. The map of engineering soil types was prepared from field observation. Mainly four types of soil domain were identified: silty gravel, low plastic clay, silty sand and clayey to silty gravel. In accordance with the unified soil classification system (ASTM D 2487-83), these domains

were named ML, CL, SM and GM to GC, respectively. The study area mainly consists of ML over the whole area. SM and CL were also recorded, but these soil types were scarce. GM to GC was found mainly on the base of hills as old fan deposits. Soils were tested in the field for soil domain classification in accordance with the field identification procedure of USBR (2001). Strength parameters for ML, SM, and GM were also estimated in the field (Figure 7) according to the methodology described by NAVFAC (1986). Soil samples were also collected to classify soil and identify the strength parameter in the laboratory and to determine in situ density, in accordance with the Japanese Industrial Standard (JIS A1225) and the Standards of the Japanese Geotechnical Society (JGS 0191). A double-ring infiltrometer (ASTM D3385-03) was used to determine the saturated infiltration rate of ML and SM. The test was conducted on concave topography of hills at the base of a pit of depth 0.5 m. Although the test is time-consuming and a huge amount of water (more than 140 litres) was used for each test, it was conducted in four locations (Figure 7). For other places, soil tubes of 100 cc were used to collect samples for a laboratory permeability test.

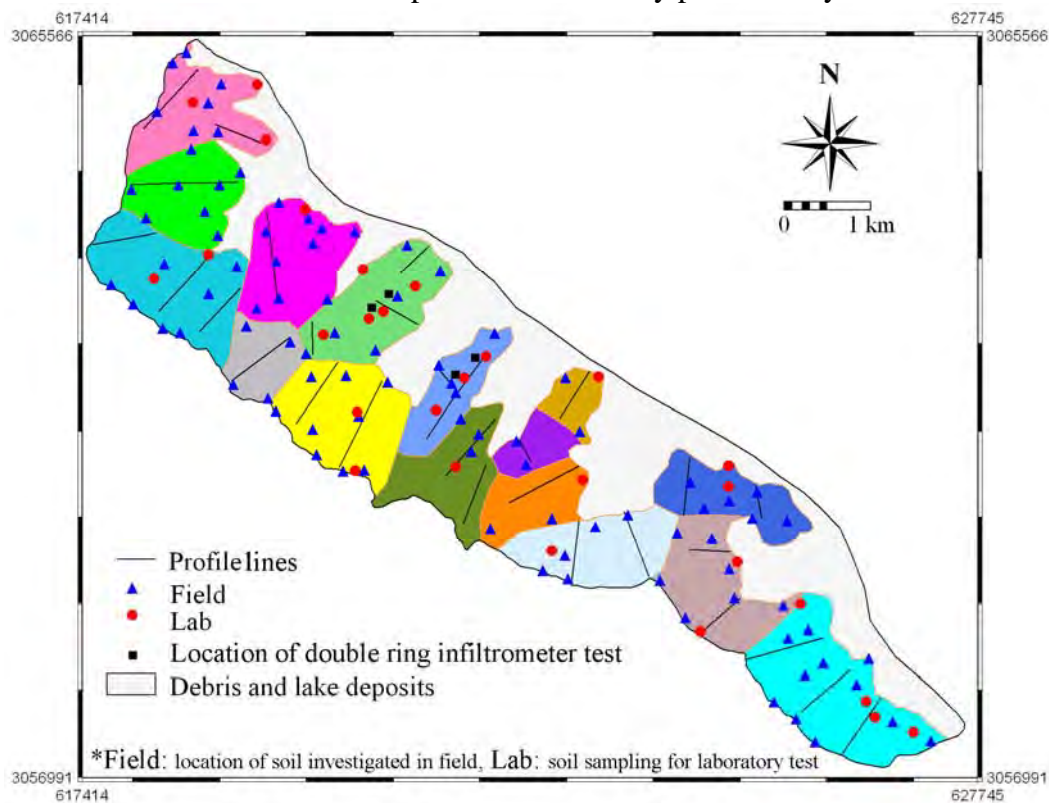


**Figure 7** Separation of 16 topo-mosaic of identical topography and selection of profile for soil depth estimation

A land use map was also prepared. Aerial photographs taken in 1996 were also used to delineate the boundaries of different land use patterns. Dense forest, dry cultivated, grassland, shrubs, sparse forest, and sparse shrubs are six domains of land use observed in the field (Figure 8). The names of plant species were also collected so that the root characteristics could be understood by consulting the published literature. *Alnus nepalensis*, *Pogonatherum paniceum*, *Schima wallichii*, *Imparata cylindrical*, *Cyperus rotundus*, *Melastoma melabathricum*, *Buddleja asiatica*, *Rubus ellipticus*, *Bidens pilosa*, *Erigeron Canadensis*, *Duranta repens*, *Carex lanceolata*, *Arunduelala nepalensis*, *Maesa chisia*, *Cymbopogon*

*microtheca*, *Eupatorium adenophorum*, *Rhododendron arboretum*, *Cryptomeria japonica*, *Lantana camera*, *Drepanostachyum intermedium*, *Berberis Asiatica*, *Quercus semecarpifolia*, *Rhododendron lepidotum* are the main plant species present in the study area. The locally protected community forest of the study area consists of immature trees, shrubs and grass.

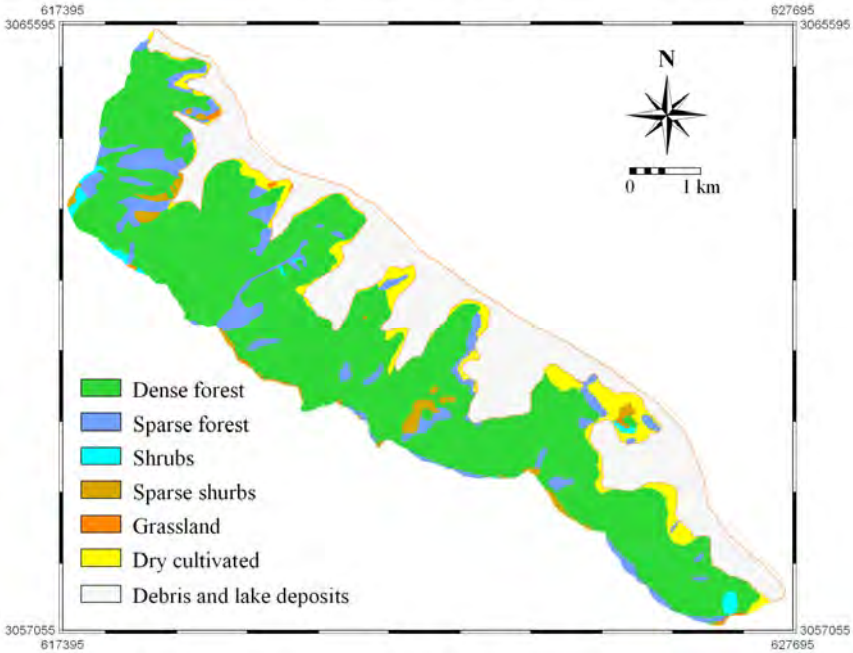


Figure 8, Landuse map used for analysis

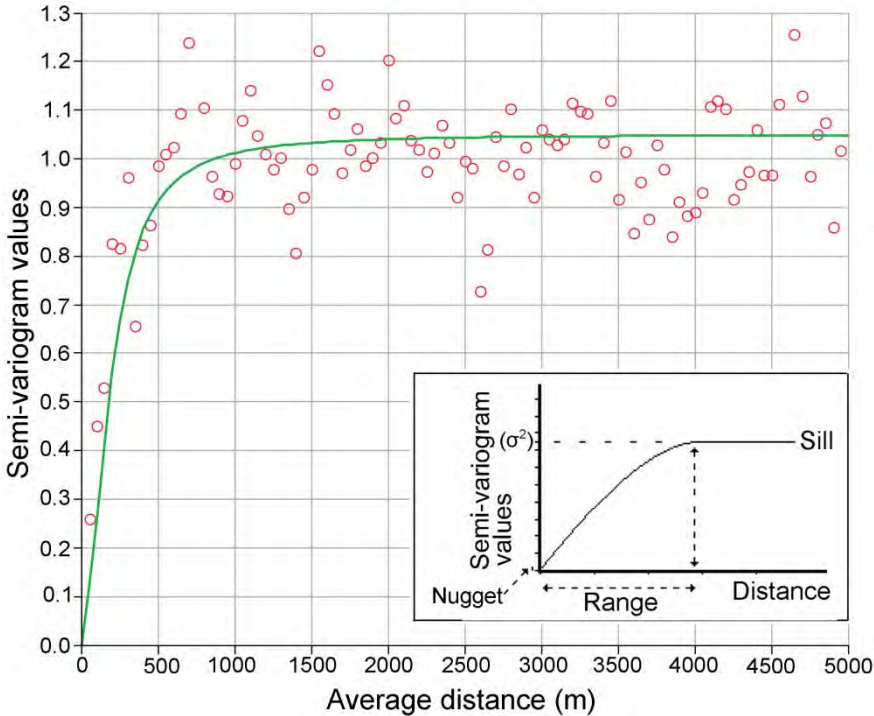
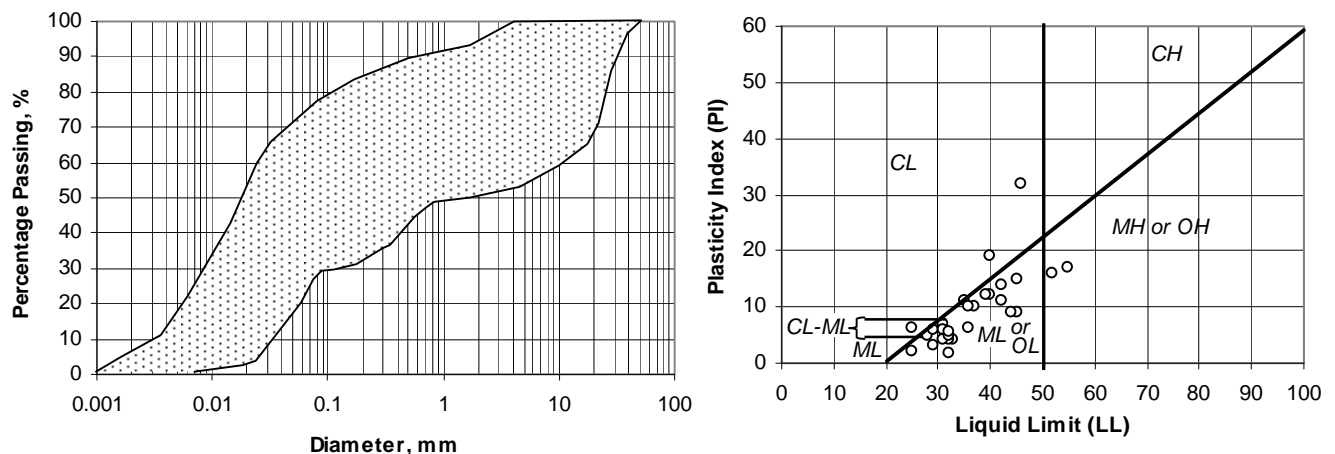


Figure 9, Rational quadratic semi-variogram model used for kriging to estimate soil depth. Inset illustrates parameters nugget, sill and range in an idealize semi-variogram model where  $\sigma^2$  is expected variance of input values.

### 3.1.3 Laboratory test

General soil mechanics tests, for such factors as grain size distribution, soil classification, plastic limit-liquid limit, bulk density, specific gravity, and unit weight were performed in the laboratory. Mainly soils from the area that was selected as an ML domain during soil mapping in the field were tested in the laboratory, because of its extensive distribution. The results show that the soil of most of the slopes is ML. This also supports the results of field soil tests. Figure 10 illustrates the grain size distribution and liquid limit – plasticity index of soils in the study area. A laboratory permeability test was also carried out according to the Japanese Industrial Standard (JIS A1218).



**Figure 10** Grain size distribution and LL-PL test results

### 3.1.4 Soil parameters

The coupled hydrological and infinite slope stability model for calculating the factors of safety described in this paper requires that some strength parameters be determined, either in the laboratory or in the field. In the main, it is necessary to determine the following parameters before running a calculation in GIS:  $C$  (soil cohesion),  $C_r$  (root cohesion),  $\phi$  (internal friction angle),  $q_0$  (vegetative surcharge),  $\gamma$  (unit weight),  $\gamma_{sat}$  (saturated unit weight),  $n$  (effective porosity), and  $k$  (hydraulic conductivity). However, it is almost impossible to determine these values for each and every slope unit. Thus, parameter values were determined from field tests, laboratory tests, and various published sources. The unit weight, angle of internal friction, effective porosity, and hydraulic conductivity of ML and SM soil domains were derived from field and laboratory test data. For CL and GM to GC domains, these values were cited from average values given by Kähenbühl and Wagner (1983).

The role played by vegetation in improving slope stability is well recognized and comprehensive reviews may be found in the literature (Gray and Leiser 1982, Greenway 1987, Morgan and Rickson, 1995; Howell 1999, Schmidt et al. 2001.). The most obvious way in which vegetation enhances slope stability is via root reinforcement. Thus, root cohesion was considered in this study because deeply penetrating vertical taproots and sinker roots provide the main contribution to the stability of slopes. A certain amount of research has been done on the root cohesion of some of the plants of the study area. Neupane (2005) estimated the tensile strength and root cohesion of *Duranta repens* and other two shrub species to assess

their potential for usage in bioengineering slope stabilization techniques. The findings of Neupane (2005) and information provided by Sidle (1991) for similar types of forest were used to estimate root cohesion for the study area. The adverse effect of vegetation for factors of safety is vegetation surcharge. Vegetation surcharge was determined on basis of the prevailing land-use pattern. The tree surcharge estimated by Kubota et al. (2004) was taken into account for estimating the vegetation surcharge of the study area. The average values of all the parameters utilized to estimate the average factors of safety are presented in [Table 2](#) and [Table 3](#).

### *3.1.5 GIS data preparation*

The study area was examined using ILWIS 3.3 software. All data available from field and laboratory study and digital data of topography were used in this slope stability modelling. A DEM with a resolution of 10 m was derived from 1:10 000 scale digital contour lines of the area. Slope and curvature maps were derived from this DEM using GIS functions. Maps of soil domain and land use were digitized and converted into raster format. The spatial distribution of the soil parameters ([Table 2](#) and [Table 3](#)) was represented as attribute maps. These attribute maps were used to calculate the average factors of safety during deterministic calculations.

The point map of soil depth prepared in the field study was also digitised. A kriging interpolation was performed to interpolate randomly distributed point values of soil depth and convert them into regularly distributed grid values. Before the interpolation, the spatial correlation of point data was investigated and autocorrelation, spatial variance and semi-variogram values were acquired. The semi-variogram values were used to obtain necessary input parameters (nugget, sill and range) for kriging by generating a rational quadratic semi-variogram model (Figure 9).

Equation (12) corresponds to the idealised slopes whose contours are coaxial circles with the same intervals and  $\varepsilon$  is the curvature of that circles. Thus, during calculation of depth of saturation according to Equations (12) and (13), the some of pixel shows higher value of saturation depth than the soil depth. To account this problem, the high value pixels are considered as totally saturated pixel for the given rainfall amount and whole soil depth of that pixel was considered as saturation depth. Likewise, the pixels having value less than zero were considered as completely dry and depth of saturation was considered as zero.

## **3.2 Deterministic analysis in GIS**

Factors of safety maps were calculated using Equations (1) and (11). Equation (11) was used to obtain the distributed saturated soil depth. The following six different scenarios of rainfall were used to obtain the saturated soil depth:

1. Return period of 2 years
2. Return period of 5 years
3. Return period of 10 years
4. Return period of 25 years
5. Recorded maximum rainfall of one day (in 2002)
6. Completely dry conditions (saturation depth 0 m)

A script was developed to calculate the depth of saturation in different scenarios of rainfall and to calculate the factors of safety maps. About 28% of the area had factors of safety less than 1 when the recorded maximum rainfall of one day (2002) was used in calculation. Likewise, when stability map was crossed with landslide map of 2002 events, out of 907 pixels of landslide scar in soil, more than 50% of landslide scar were in the unstable pixels. There are a few pixels (0.8%) that are still unstable although conditions were dry (no rainfall). In this respect, this calculation is prone to error. Such unstable yet dry areas are found to be concentrated in comparatively steep slope and localities of thin soil cover. Probably, vegetation cover (root strength) has an effect that the calculation cannot accommodate. The average values of soil parameters and vegetation were used to calculate the factors of safety because of natural variability and the comparatively large extension of the study area. This leads to some sort of uncertainty in the estimated factors of safety maps. Thus, probability analysis was carried out with respect to variation in soil parameters and average factors of safety maps, to obtain relatively accurate failure probability maps.

#### 4 Failure probability maps

The input parameters of soil and vegetation contained some degree of uncertainty. This kind of method of calculating FS needs to be checked for error. There are a number of methods by which the propagation of error may be analysed. Such methods are well recognized and comprehensive reviews may be found in the literature (Ward et al. 1981, Terlien 1996, Hammond et al., 1992, Burrough and McDonnell 1998). The use of safety factors calculated from average values is not recommended (van Westen and Terlien 1996). In particular,  $C$ ,  $C_r$  and  $Tan\phi$  can be quite variable from point to point in a soil mass, whereas  $\gamma_{sat}$  and  $\gamma$  are less variable (Ward et al. 1981). All calculations were pixel-based, so variation of the slope angle  $\beta$  is not possible because it was calculated from a DEM of 10 m resolution. These assumptions produce a linear relationship of Equation (1) for factors of safety.

$$FS = \alpha_1 C + \alpha_1 C_r + \alpha_2 Tan\phi \dots\dots\dots (14)$$

Where

$$\alpha_1 = \frac{1}{B Sin\beta Cos\beta} \text{ and } \alpha_2 = \frac{A Cos\beta}{B Sin\beta}$$

The values of A and B are given in Equations (2) and (3). The expected or mean of linear Equation (12) can be expressed as follows (Ward et al. 1981, Ross 2004):

$$E[FS] = \alpha_1 E[C] + \alpha_1 E[C_r] + \alpha_2 E[Tan\phi] \dots\dots\dots (15)$$

Where  $E[\cdot]$  is the expected value of the enclosed variable. In fact,  $E[FS]$  is the average factor of safety and it was calculated in the forms of maps in an earlier section. If the strength parameters are not correlated significantly between point to points and between themselves, the variance of FS can be written as follows (Ward et al. 1981; van Westen and Terlien 1996; Ross 2004):

$$V[FS] = \alpha_1^2 V[C] + \alpha_1^2 V[C_r] + \alpha_2^2 V[Tan\phi] \dots\dots\dots (16)$$

Where  $V[\cdot]$  is the variance of the enclosed variable. Equation (16) is a relatively simple formula for error propagation, which only takes into account the variance of parameters  $C$ ,  $C_r$  and  $Tan\phi$ . When Equation (14) is used in GIS, it gives a variation map of the factors of safety in terms of the variation of  $C$ ,  $C_r$  and  $Tan\phi$ .

The variations of  $C$ ,  $C_r$  and  $Tan\phi$  are required to calculate the variance of FS. In our study, the variance of  $\phi$  was estimated from the range of values determined in the field by the method described by NAVFAC (1986). The values of  $C$  and  $C_r$  need extensive measurements, which lies beyond the scope of this research. Thus, their variables were considered to fall within a certain realistic range and were assumed to be uniformly distributed random values. Information provided by Kähenbühl and Wagner (1983), Sidle (1991) and Neupane (2005) was considered when selecting the uniformly distributed random values. Thus, the variance of such a random value was calculated as follows (Ward et al., 1981):

$$V[X] = \frac{(X_{max} - X_{min})^2}{12} \dots\dots\dots (17)$$

Where  $X_{max}$  and  $X_{min}$  are the maximum and minimum of the random values on variable  $X$ . An assumption of the uniform distribution of the values of  $C$  and  $C_r$  can represent a realistic range of input values. However, it may overestimate the variance, because there is a higher chance of low values of  $C$  and  $C_r$  in each pixel. The calculated value of variance is given in **Table 4**.

Considering that the average factors of safety have a normal distribution, the deviation from  $F = 1$  (limit of stability) can be calculated in the form of a  $Z$  score or  $Z$  value. The standardized  $Z$  score has a zero mean and its deviation from the mean is expressed in standard deviations. The area under the standardized normal distribution can be expressed directly as a probability (Ross 2004). The normal distribution curve of the  $Z$  score helps when calculating the failure probability. The following formula was used to calculate the  $Z$  score from average factors of safety and variance of factors of safety:

$$Z = \frac{FS - E[FS]}{\sqrt{V[FS]}} \dots\dots\dots (18)$$

Where  $FS$  is the limit value of factors of safety ( $FS = 1$ ). The square root of variance of factors of safety can be also expressed in terms of standard deviation. Thus, Equation (18) gives the following relationships:

$$Z = \frac{1 - E[FS]}{S[FS]} \dots\dots\dots (19)$$

Where  $S[FS]$  is the standard deviation of factors of safety.

The failure probability is equal to the area under the standardized normal distribution between the  $Z$  score for  $F = 1$  and  $Z = -\infty$ . The area under the standardized normal distribution can be found in tables available in any statistical handbook. However, for large amount of data, as in this study, commercially available spreadsheet software can be used to calculate the probability from the  $Z$  value. Details of the procedure of error propagation and calculation of failure probabilities are summarized by Terlien (1996) and van Westen and Terlien (1996).

The probability value calculated outside GIS was imported in GIS and failure probability maps of various scenarios were prepared. Examples of the failure probability map of 2-years and 25-years return period are provided in **Figure 10**. The failure probability maps of all scenarios were analysed in terms of the change in percentage area coverage with respect to the return period of various amounts of rainfall (**Figure 11**). Plotted data show that probability of failure from 1% to 25% changes abruptly to an area with a higher probability of failure (50%

to 100%) when the amount of rainfall increases from a less to a high return period, because of the strong role of saturated soil depth in factors of safety.

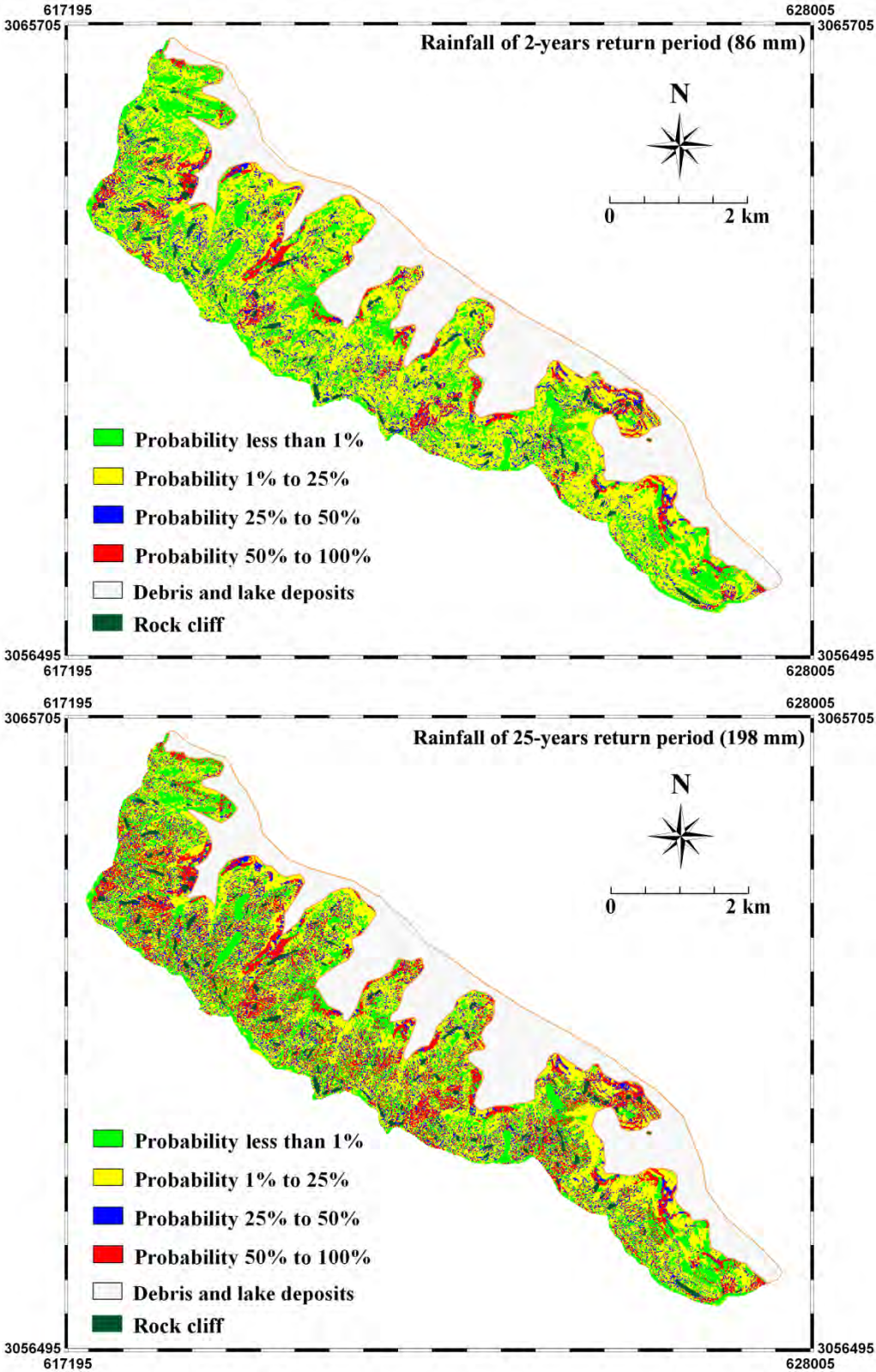


Figure 11 Failure probability maps in scenario of rainfall of 2 and 25 years return period

### 5 Discussion and conclusions

The accuracy of probability maps must be checked against prevailing landslide scenarios. Thus, the probability map calculated from the rainfall amount of 2002 was checked against the actual occurrences of landslides. A map showing the distribution of landslides after the 2002 rainfall events is available (Paudyal and Dhital, 2005; Dahal et al. 2008). The authors also prepared landslide maps, excluding deposition and transportation zone, during field visits in the years 2003, 2005 and 2006. Both maps were combined and final landslide (only failure scar) raster maps were prepared in GIS. This resulting map was overlain with a hazard map (Figure 12). A total of 73 landslides occurred in the study area after the extreme rainfall of July 23, 2002. Landslide scars occupied only 1084 pixel (0.60%) of the total study area. Out of 1084 pixels of landslide scar, 177 pixels of landslide scars were noticed on rocky cliff, thus only 907 pixels were considered to analyse accuracy of hazard map. The raster map of landslide scars was crossed with the failure probability map of 2002 rainfall. The result shows that a total of 50.3% of the landslide pixels show a probability of 50% to 100% (Figure 13). Similarly, 17.3% of the landslide pixels show a probability of 25% to 50%. Likewise, 20% of the pixels show a failure probability of 1% to 25%, while 12.5% of the landslide pixels show a probability of less than 1%. In comparison to the total landslide area, these results are quite encouraging, because it is not required that all landslide pixels have a high probability value (van Westen and Terlien, 1996).

The resultant failure probability value can suggest the probability of slope failure in the study area during extreme rainfall events. However, these factors of safety values and the probability of failure need to be considered as symptomatic values of translational slides (Varnes 1984) only. Moreover, the saturated depth of soil estimated by the model described by Iida (1984) is a theoretical one-dimensional model of through flow and considered slope concavity. Although it does not consider slope length, its usage in GIS-based infinite slope stability analysis is quite promising.

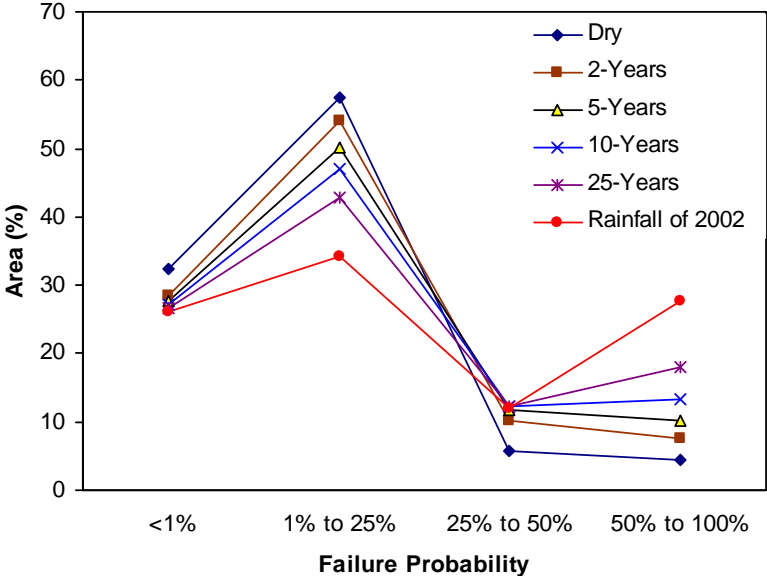


Figure 12 Slope failure probability in different scenario of rainfall. Figure shows that failure probability 1% to 25% abruptly change to 50% to 100% failure probability in increasing amount of rainfall

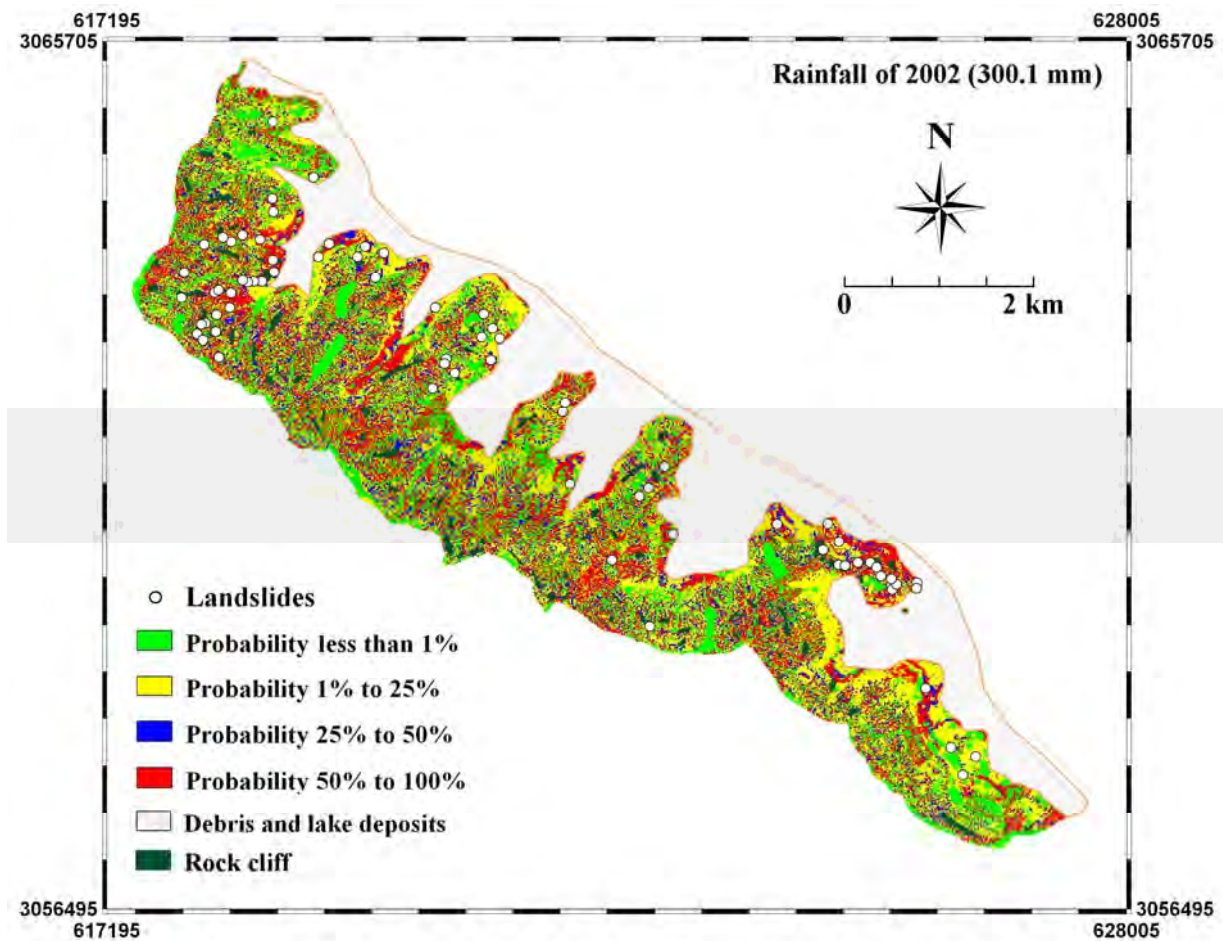


Figure 13, Probability map prepared for 2002 rainfall crossed with landslide distribution maps prepared after disaster event of 2002

The failure probability calculated in the study addresses only hill slopes. The current practice of settling on the plain area immediately after the base of the hills may need to be evaluated by taking into account the probability of slope failure on the up-hill sections. The resultant failure probability map can be checked against the statistical landslide hazard zonation map. Finally, as mentioned by van Westen and Terlien (1996) and van Westen (2000), there are some limitations in this kind of study, but the results can be used with landslide distribution maps and hazard maps to evaluate the area for settlement.

There is high demand for research into probability of failure and landslide hazard zonation in the Lesser Himalayan slopes of Nepal and this research is an attempt of analysing the Lesser Himalayan slopes of Nepal in terms of deterministic hazard analysis. A greater area needs to be evaluated for failure probability, which will help in the preparation of local-level failure probability maps that can be used for sustainable development and planning in the Himalayan region.

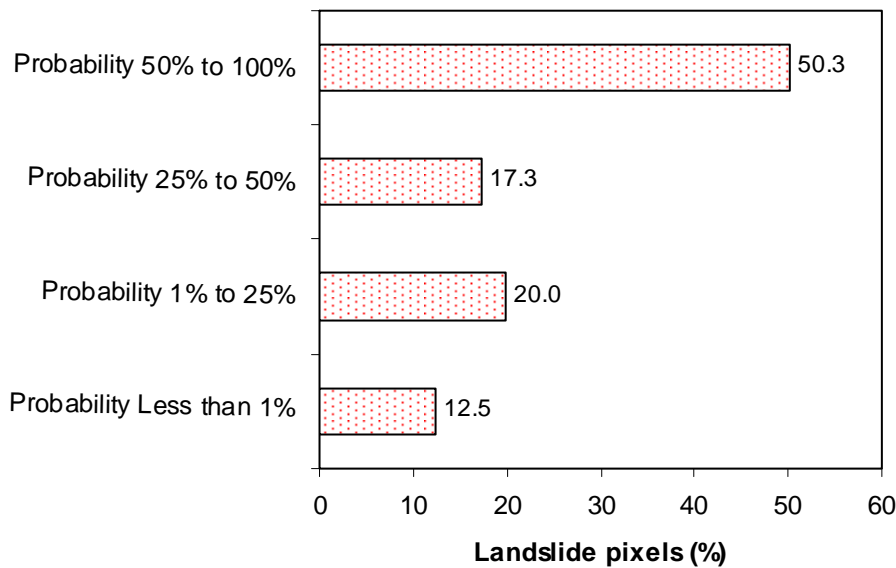


Figure 14, Comparison of calculated failure probability with existing landslides triggered by 2002 rainfall events

### Acknowledgements

We thank local community forest users groups for providing permission to enter the forest for investigation. We sincerely acknowledge Dr. Netra Prakash Bhandary for his comments and suggestions. We thank Mr. Anjan Kumar Dahal and Ms. Seiko Tsuruta for their technical support during the preparation of this paper. The study has been partly funded by the Sasakawa Fund for Scientific Research, The Japan Science Society.

### References

- Acharya, G., De Smedt, F. and Long N.T., 2006. Assessing Landslide hazard in GIS: a case study from Rasuwa Nepal, *Bull eng Geol Env*, 65, 99-107.
- Acharya, K.K., 2001. *Geology and structure of the Pharping – Raniban area central Nepal*, M. Sc. Thesis, Central Department of Geology, Tribhuvan University, p. 58.
- ASTM D 2487-83 Standard classification of soils for engineering purposes (Unified Soil Classification System), ASTM International, 100 Bar, harbor Drive, west Conshohocken, PA 19428, USA
- ASTM D3385-03 Standard test method for infiltration rate of soils in field using double-ring infiltrometer, ASTM International, 100 Bar, harbor Drive, west Conshohocken, PA 19428, USA
- Beven, K.J. and Kirkby, M. J. 1979. A physical based variable contributing area model of basin hydrology, *Hydrological sciences Bulletin*, 24 (1), 43-69
- Borga, M., Dalla, F.G., Da Ros, D. and Marchi, L. 1998. Shallow landslide hazard assessment using a physically based model and digital elevation data. *Environmental Geology*, 35(2-3), 81-88
- Borga, M., Dalla, F.G, Gregoretti, C. and Marchi, L. 2002. Assessment of shallow landsliding by using a physically based model of hillslope stability, *Hydrol. Processes*, 16, 2833-2851.
- Burrough, P.A. and McDonnell, R.A., 1998. *Principles of Geographical Information Systems*, Oxford Univ Press, p. 333
- Burton, A. and Bathurst, J.C. 1998. Physically based modeling of shallow landslide yield at a catchment scale, *Environmental Geology*, 35(2-3), 89-99.

- Can, T., Nefeslioglu, H.A., Gokceoglu C., Sonmez H., Duman T.Y. 2005. Susceptibility assessments of shallow earthflows triggered by heavy rainfall at three catchments by logistic regression analyses, *Geomorphology*, 72, 250-271.
- Crozier, M.J. 1999. Prediction of rainfall-triggered landslides: a test of the antecedent water status model. *Earth Surface Processes and Landforms*, 24, 825– 833.
- Cruden, D.M. and Varnes, D.J. 1996. Landslide types and processes. In: Turner, A.K. and Schuster, R.L. (Eds), *Landslides: Investigation and Mitigation. Sp. Rep.247*, Transportation Research Board, National Research Council, National Academy Press, Washington D.C., pp. 36-75.
- Dahal, R.K., Hasegawa S. 2008. Representative rainfall thresholds for landslides in the Nepal Himalaya, *Geomorphology* (in press), doi:10.1016/j.geomorph.2008.01.014.
- Dahal, R. K., Hasegawa, S. Nonomura, A., Yamanaka, M., Dhakal, S., Poudyal, P. 2008. Predictive modelling of rainfall induced landslide hazard in the Lesser Himalaya of Nepal based on weights-of-evidence, *Geomorphology* (in press), doi: 10.1016/j.geomorph.2008.05.041.
- Dahal, R.K., Hasegawa, S., Yamanaka, M. and Nishino, K. 2006. Rainfall triggered flow-like landslides: understanding from southern hills of Kathmandu, Nepal and northern Shikoku, Japan. *Proc 10th Int Congr of IAEG, The Geological Society of London*, IAEG2006 Paper number 819, 1-14 (CD-ROM).
- Dahal, R.K. and Kafle, K.R. 2003. Landslide Triggering by torrential rainfall, understanding from the Matatirtha landslide, south western outskirts of the Kathmandu valley, In: *Proceedings of one day International seminar on Disaster mitigation in Nepal*, Nepal Engineering College and Ehime University, pp. 44–56.
- Dietrich, W.E., Reiss, R., Hsu, M. and Montgomery, D.R. 1995, A process-based model for colluvial soil depth and shallow landsliding using digital elevation data. *Hydrological Processes*, 9, 383–400.
- Duncan, M.J., 1996. Soil slope stability analysis. In: Turner, A.K., Schuster, R.L., (Eds.), *Landslides: investigations and mitigation. Special Report, vol. 247*. Transportation Research Board, National Research Council, Washington, pp. 337–371.
- Duzgun, H.S.B., Karpuz, C. 2003. GIS-Based Landslide Risk Assessment for Bandirma Harbor, *12th Panamerican Conference on Soil Mechanics and Geotechnical Engineering, Massachusetts Institute of Technology, Cambridge, USA, vol.1*, pp. 2803-2810.
- Eaglin, R., 1996. DISTRIB 2.13 for Windows for statistical distribution analysis, the accompanying software in the textbook *Water Quantity and Quality Control*, 2nd Edition John Wiley and Sons publishers, p. 592.
- Glade, T., Crozier, M. and Smith, P. 2000. Applying probability determination to refine landslide-triggering rainfall thresholds using an empirical Antecedent Daily Rainfall Model, *Pure and Applied Geophysics* 157, 1059– 1079.
- Gökceoglu, C. and Aksoy, H. 1999. Landslide susceptibility mapping of the slopes in the residual soils of the Mengen region (Turkey) by deterministic stability analyses and image processing techniques, *Engineering Geology* 44, 147-161.
- Graham, J. 1984. Methods of stability analysis, in Brunsden, D. and Prior, D. B. (Eds), *Slope Instability*, Wiley and Sons, New York, pp. 171-215.
- Gray, D.H. and Leiser, A.T. 1982. *Biotechnical slope protection and erosion control*. Van Nostrand Reinhold, New York
- Greenway, D.R., 1987. Vegetation and slope stability. In: Anderson MG, Richards KS (eds.) *Slope stability*. Wiley, New York, pp 187–230

- Hammond, C., Hall, D., Miller, S. and Swetik, P. 1992. Level I Stability analysis (LISA), *Documentation for Version 2.0, Gen. Tech. Rep. INT-285*, Ogden, UT: U.S. Department of Agriculture, Forest Service, Intermountain Research Station, p. 190.
- Howell, J., 1999. Roadside Bio-engineering, HMG Nepal, Department of Roads, Babar Mahal, Kathmandu, Nepal, Reference Manual 216p and Site Handbook, p. 160.
- Iida, T., 1984. A hydrological method of estimation of the topographic effect on the saturated throughflow. *Trans. Japanese Geomorph. Union*, 5, 1–12 (in Japanese with English abstract)
- Iida, T. 1999. A stochastic hydro-geomorphological model for shallow landsliding due to rainstorm, *Catena* 34, 293–313
- Iverson, R.M., 2000, Landslide triggering by rain infiltration, *Water Resources Research*, 36(7), 1897-1910.
- Kähenbühl, J. and Wagner, A., 1983. *Survey, design and construction of trail suspension bridge for remote areas, Vol. B (survey)*, SKAT, Swiss Centre for Appropriate Technology, Varnbühlstrasse 14, 9000 St. Gallen, Switzerland, p. 325.
- Kubota, T., Omura, H., Okumura, T., Tada, Y. and Paudel, P.P., 2004. Influence of the forest tree load on the slope stability with different forest felling, *Journal of the Japan Landslide Society* 41(3), 273-281 (in Japanese with English abstract).
- Lamb, R., Beven, K.J. and Myrabo, S., 1998. A generalized topographic-soil hydrological index. In: *Landform Monitoring, modelling and Analysis*, Lane, S., Richard, K. and Chandler, J. (eds.). Wiley: Chichester pp. 263–278.
- Montgomery, D.R. and Dietrich, W.E., 1994. A physical based model for the topographic control on shallow landsliding, *Water Resources Research*, 30(4), 1153–1171.
- Morgan, R.P.C. and Rickson, R.J. 1995. *Slope stabilization and erosion control*. E and FN Spon: London, p. 274.
- NAVFAC, 1986. *Design manual: soil mechanics*, U.S. Dept of Defense, NAVFAC DM-7.01, Department of the Navy, Washington DC, revised version, p. 389.
- Neupane, R.R., 2005. *Experimental analysis of strength of local grass and shrub roots used for slope stabilization*, Thesis No. 059/MSW/418, Master of Science in Water Resources Engineering, Institute of Engineering, Tribhuvan University, Nepal, p. 85.
- Okimura, T. and Kawatani, T., 1987. Mapping of the potential surface-failure sites on granite mountain slopes. In: Gardiner, V. (ed) *Int Geomorp Part I*. Wiley, New York, pp. 121–138.
- Onda, Y., 1992. Influence of water storage capacity in the regolith zone on hydrological characteristics, slope processes and slope form. *J. Geomorph. N. F.*, 36, 165-178
- Pack, R.T., Tarboton, D.G. and Goodwin, C.N., 1998. *SINMAP, A stability index approach to terrain stability hazard mapping*, Users Manual (available at <http://www.tclbc.com>), Utah State University, Terratech Consulting Ltd., Canadian Forest Products Ltd, C.N. Goodwin Fluvial System Consulting, p. 68.
- Pack, R.T., Tarboton, D.G. and Goodwin, C.N., 2001. SINMAP approach to terrain stability mapping. In: Moore DP and Hungr O (eds.), *Proceedings of International Conference of International Association for Engineering Geology and the Environment*, AA Balkema, Rotterdam, Netherlands: pp. 1157-1165.
- Paudel, P.P., Omura, H., Kubota, T. and Morita, K., 2003. Landslide damage and disaster management system in Nepal. *Disaster Prevention and Management*, 12(5), 413-419.
- Paudyal, P. and Dhital, M.R., 2005. Landslide hazard and risk zonation of Thankot – Chalnakhel area, central Nepal, *Journal of Nepal Geological Society*, 31, 43-50.

- Ross, S.M., 2004. *Introduction to probability and statistics for engineers and scientists*, third edition, Academic press (an imprint of Elsevier), Elsevier Delhi, India, p. 624.
- Schmidt, K.M., Roering, J.J., Stock, J.D., Dietrich, W.E., Montgomery, D.R. and Schaub, T., 2001. The variability of root cohesion as an influence on shallow landslide susceptibility in the Oregon Coast Range, *Can. Geotech. J.*, 38, 995–1024.
- Sidle, R.C. 1991. A conceptual model of changes in root cohesion in response to vegetation management, *Journal of Environmental Quality*, 20(1), 43-52.
- Skempton, A.W. and DeLory, F.A. 1957, Stability of Natural slopes in London Clay, *ASCE Journal* 2:378-381
- Soeters, R. and van Westen, C. J., 1996. Slope Instability Recognition, Analysis and Zonation, In: Turner A K, Schuster RL (eds.) *Landslides, investigation and mitigation*, Transportation Research Board, National Research Council, Special Report 247, National Academy Press, Washington D.C., U.S.A., pp. 129–177.
- Stöcklin, J. and Bhattarai, K.D., 1977. Geology of Kathmandu Area and Central Mahabharat Range Nepal Himalaya Kathmandu. HMG/UNDP Mineral Exploration Project, Technical Report, New York, p. 64.
- Stöcklin, J. 1980. Geology of Nepal and its regional frame, *Journal of the Geological Society London*, 137, 1-34.
- Terlien, M.T.J., van Asch Th, W.J. and van Westen, C.J., 1995. Deterministic modelling in GIS-based landslide hazard assessment, In: Carrara, A. and Guzzetti, F., Eds. *Advances in Natural and Technological Hazard Research*, Kluwer, pp. 51-77.
- Terlien, M.T.J. 1996. *Modelling spatial and temporal variations in rainfall-triggered landslides*, PhD thesis, ITC Publ. Nr. 32, Enschede, The Netherlands, p. 254.
- Uchida, T., Kataoka, S., Iwao, T., Matsuo, O., Terada, H., Nakano, Y., Sugiura, N., and Osanai, N. (2004) A study on methodology for assessing the potential of slope failures during earthquakes, Technical note of National Institute for Land and Infrastructure Management, Japan, pp 91 (in Japanese).
- USBR, 2001. *Engineering geology field manual*, second edition Vol I, U.S. Department of the Interior Bureau of Reclamation, p. 432.
- van Westen, C.J., 2000. The modelling of landslide hazards using GIS, *Survey in Geophysics*, 21, 241-255.
- van Westen, C.J. and Terlien, T.J., 1996. An approach towards deterministic landslide hazard analysis in GIS. A case study from Manizales (Colombia). *Earth Surf Proc Landforms* 21:853–868
- Varnes, D. J., 1984. Landslide Hazard Zonation: a review of principles and practice, Commission on landslides of the IAEG, UNESCO, *Natural Hazards* 3, pp. 61.
- Wanielista, M.P., Kersten, R. and Eaglin R., 1996. *Water Quantity and Quality Control*, 2nd Edition with computer program SMADA 6.43, John Wiley and Sons publishers. 592p.
- Ward, T.J., Li, R-M. and Simons, D.B., 1981. Use of a mathematical model for estimating potential landslide sites in steep forested basin, In: Davis, T.R.H., Pearce, A.J., eds. *Erosion and sediment transport in pacific Rim steep lands*, International hydrological Science Publ No. 132, Institute of Hydrology, Wallingford, Oxon, UK, pp. 21-41.
- Wu, W. and Sidle, R.C., 1995. A distributed slope stability model for steep forested basins, *Water Resour Res*, 31, 2097–2110.
- Xie, M., Esaki, T. and Cai, M., 2004. A time-space based approach for mapping rainfall-induced shallow landslide hazard, *Environmental Geology*, 46, 840-850.